Total Solar Eclipse Observations: A Treasure Trove from the Source and Acceleration Regions of the Solar Wind

Journal of Physics: Conference Series **1620** (2020) 012006 doi:10.1088/1742-6596/1620/1/012006

Total Solar Eclipse Observations: A Treasure Trove from the Source and Acceleration Regions of the Solar Wind

Shadia Rifai Habbal

Institute for Astronomy, University of Hawaii, Honolulu, Hawaii 96822, USA

E-mail: habbal@hawaii.edu

Abstract.

A comprehensive exploration of the *inner corona*, namely the spatial span starting from the solar surface out to a few solar radii, is essential for investigating the physical processes responsible for its quiescent and dynamic state. Such an exploration encompasses the source regions of the solar wind, and is thus essential for reliably establishing their link to in-situ measurements, including those from the more recent Parker Solar Probe mission. Total solar eclipses are the only platform available at present to fulfill these requirements, as they offer a spatially uninterrupted diagnosis of the inner corona through multi-wavelength imaging and spectroscopy. This review highlights results from almost two decades of eclipse observations. Particular emphasis is placed on the discovery of the complexity of coronal structures, in particular at the source regions of the solar wind, directly connected to prominences. Complex structures include different manifestations of waves and plasma instabilities. Imaging in coronal emission lines yields the only diagnostic tool, known to date, for the empirical inference of the freeze-in distance of heavy ions. Imaging also enables the mapping of the electron temperature in the inner corona, and its changes in response to the passage of a coronal mass ejection (CME). Furthermore, spectroscopic observations reveal that cool prominence material associated with a CME, travels in tandem, unscathed, into interplanetary space. Multi-wavelength imaging and spectroscopy during total solar eclipses thus yield a treasure trove from the sources and acceleration regions of the solar wind, which beg continued exploitation in search of signatures of coronal heating and solar wind acceleration processes.

1. Introduction

It is an often forgotten fact that total solar eclipse observations led to fundamental discoveries in solar and heliospheric physics. The example of the 7 August 1869 total solar eclipse is a particularly relevant one. Using the recently invented spectrograph, Young (1870, 1871, 1872) observed a bright 'greenish' spectral line (see Figure 1) whose wavelength had no counterpart in catalogs of spectral lines known at the time. It took almost 70 years before Grotrian (1939) and Edlén (1945) identified this 'coronium' line as emission from Fe^{+13} at 530.3 nm, currently known as Fe XIV. This discovery implied that the temperature of the coronal atmosphere exceeded a million degrees, and was thus fully ionized. A decade later, Parker (1958) demonstrated theoretically that a hot corona could not remain bound to the Sun, but would expand into interplanetary space. E N Parker called this supersonic expansion *the solar wind*, whose existence was subsequently confirmed in *in situ* measurements by Neugebauer and Snyder (1966). A

hot corona also implied that emission from the solar disk as well as off the limb at shorter
and x-rays, could be observed from space over
s paved the way for a new era of exploration

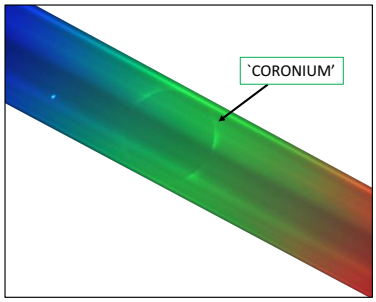

Figure 1. Total solar eclipse slitless spectrum of the corona taken by M. Druckmüller. The spectrum is centered on the green 'coronium' line, currently known as Fe XIV 530.3 nm.

Lyot's invention of the coronagraph (Lyot 1932), was instigated by the limited opportunities afforded by total solar eclipses to observe the corona. This major technological breakthrough enabled daily coronal imaging with high temporal cadence, as successfully demonstrated with several years of polarimetric observations in the Fe XIII 1074.7 nm and Fe XIV 530.3 nm lines from Sac Peak Observatory (Arnaud and Newkirk 1987), and decades of white light imaging from space with the SOHO/LASCO C2 and C3 coronagraphs (Brueckner et al. 1995).

However, despite the current proliferation of ground and space-based observatories for remote exploration of the corona, this review highlights how total solar eclipse observations in the visible spectral range, including the near infrared, continue to yield key insights into the properties of the corona and of the sources of solar wind streams, untenable at present by other observing platforms.

2. The highly structured and dynamic corona

Broad-band continuum emission in the visible, commonly referred to as white light, is produced by the scattering of photospheric radiation by free electrons and dust streaming through the corona. Application of advanced image processing techniques to high resolution photographic and digital eclipse images, developed by M Druckmüller (Druckmüller et al. 2006, Druckmüller 2009), has further unveiled hidden details within these structures, spanning sub arcsecs to several solar radii spatial scales, as shown in the examples of Fig. 2.

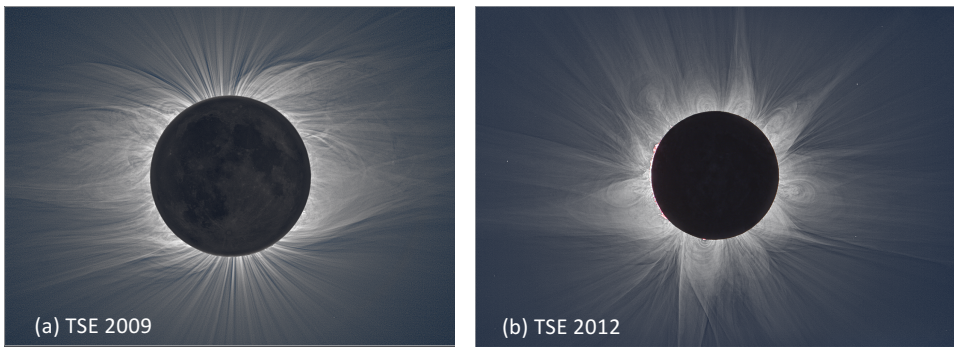

Figure 2. Processed white light images of the corona from the total solar eclipses of (a) 22 July 2009, taken from Enewetak Atoll in the Marshall Islands by P. Aniol, and (b) 14 November 2012, taken by C. Emmanouilidis from Queensland, Australia.

Taken at solar minimum on 2009 July 22 (Fig. 2a), and solar maximum on 14 November 2012 (Fig. 2b), the ubiquity of the fine scale coronal structures in these images underlines the difference in the distribution of the larger scale structures as a function of phase within a solar cycle. At solar minimum (Fig. 2a), the polar regions are clearly defined by expanding *open* field structures, while streamers mostly occupy the equatorial plane. At solar maximum (Fig. 2b), streamers are almost regularly distributed around the solar disk. In both cases, however, open field lines dominate the corona, while *closed*, often complex, arch-like structures are limited to the bulge of streamers, which extend to much greater heights at solar minimum than at solar maximum. While the realization that the *shape* of the corona changes as a function of solar cycle dates back to at least the 19th century (see Maunder 1899), the novelty of the (representative) examples of Fig. 2 is the presence of a plethora of complex structures, independently of the phase within the solar cycle. These complex structures reflect the dynamic component of the expanding coronal plasma, and are, in essence, tracers of the magnetic field lines. This was recently demonstrated by Boe et al. (2020b) who inferred the topology of the coronal magnetic field by applying the Rolling Hough Transform (RHT) (Clark et al. 2014) to processed white light eclipse images. As illustrated in the example of Fig. 3, the technique captures the departure of the magnetic field direction from radial expansion. The inferred angle relative to radial is shown in Fig. 3D. The technique also captures the complexity of the field within the bulges of the streamers, as evident in Fig. 3C,D.

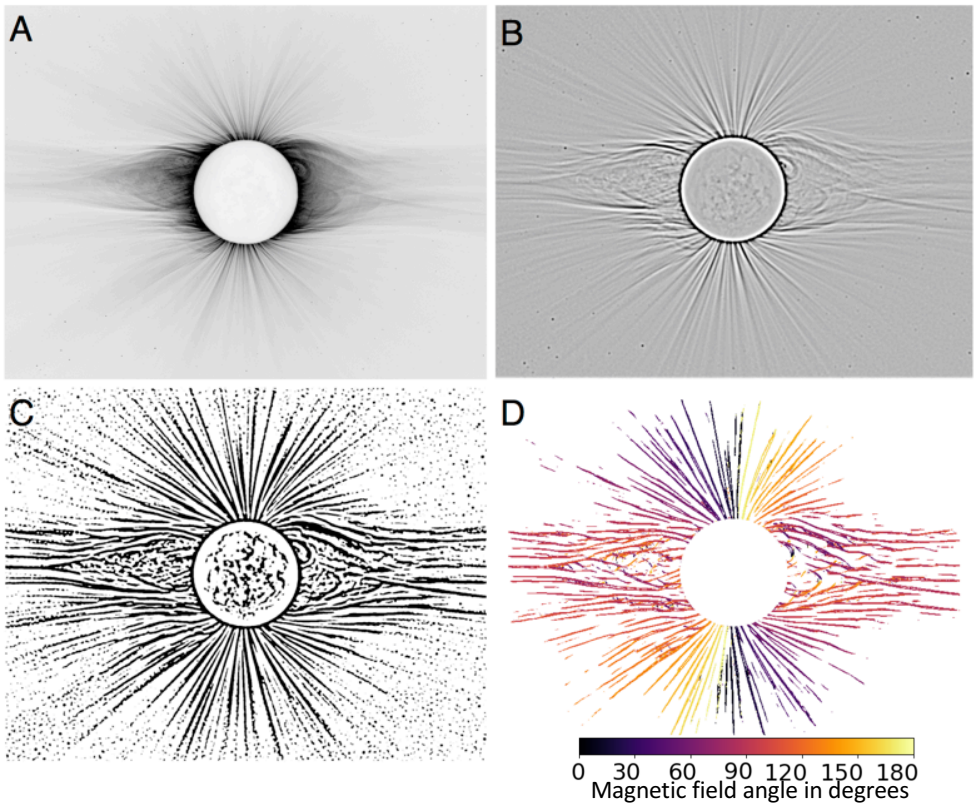

Figure 3. Results of the application of the RHT procedure to the 2019 total solar eclipse processed white light image (A, where the brightest features are black). A high-pass filter is applied to A, which is then blurred (B) and converted to a binary image (C). The RHT algorithm is then applied to C, resulting in the colored image D, with the angle of the magnetic field relative to radial given by the color coding shown below. (See Boe et al. 2020b for details.)

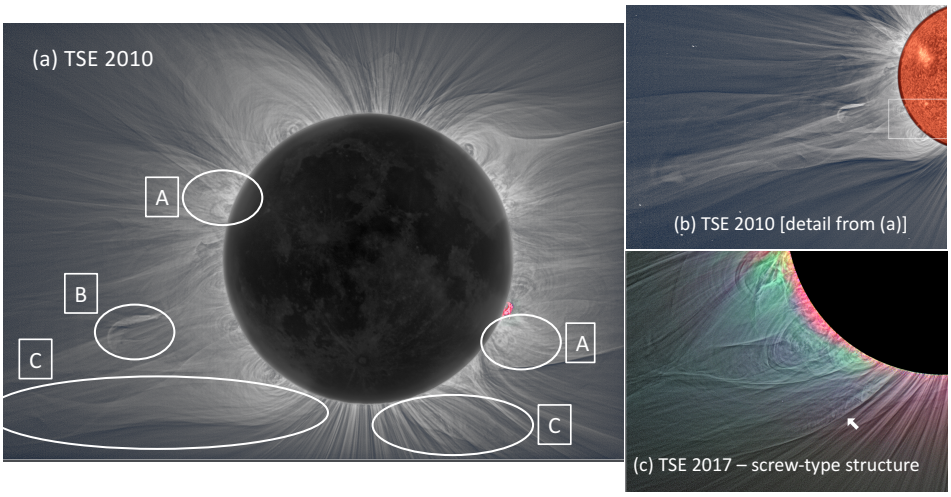

Figure 4. (a) Total solar eclipse white light image from 2 July 2010, with different structures akin to plasma instabilities (A), and wavy patterns (B,C). (b) Details of the south east large amplitude wave shown in (a). (c) Corkscrew-type wavy motion from the 21 August 2017 eclipse (red is Fe XI emission, green is Fe XIV emission).

As a matter of fact, this complexity is ubiquitous in all white light eclipse images; it appears in the form of turbulent-like structures akin to plasma instabilities, spanning a range of spatial scales, as shown encircled by ovals A in Fig. 4a. In addition, large-scale helical structures are also invariably captured in eclipse images, such as feature C in Fig.4a,b. A corkscrew-type wavy motion is captured in Fig. 4c (see arrow). All these features are invariably associated with quiescent and erupting prominences anchored at the base of the corona, with or without the occurrence of a CME (see Druckmüller et al. 2014 for details.)

Another ubiquitous property of prominences is their appearance within a shroud of hot large scale loops, as shown in Fig. 5A. The temperature signature is from the Fe XIV emission at 1.8 MK, shown in green in this panel. In white light images, on the other hand, the connectivity between the filamentary structures within prominences and the filaments forming the overlying coronal arch-like structures is also indelible, as shown by the white arrows in Fig. 5B.

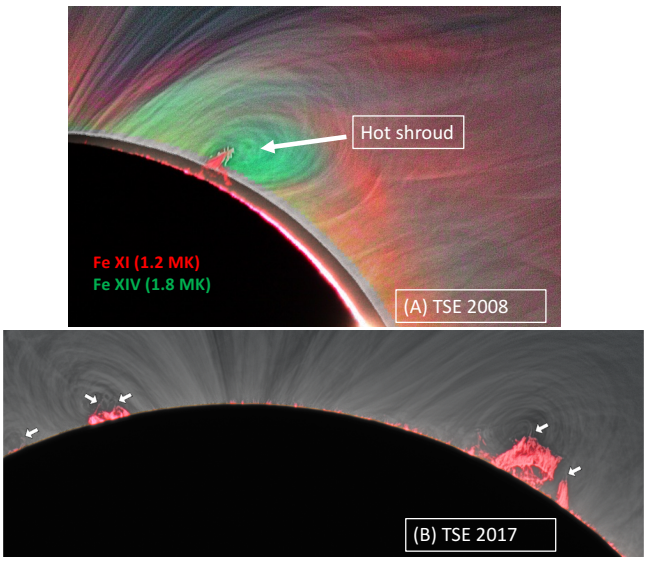

Figure 5. (A) Hot prominence shroud of (green) Fe XIV 530.3 nm (1.8 MK) emission surrounding a large prominence seen in Hα emission. Red is emission from Fe XI 789.2 nm (1.2 MK). (B) Connectivity between filaments within prominences and surrounding coronal structures.

On the other hand, details of large-scale features are equally striking in the two examples of Fig. 6 from the 2012 and 2013 eclipses taken at solar maximum (see Alzate et al. 2017 for details). The serendipitous occurrence of CMEs during these eclipses enabled the study of their imprints, as indicated by the yellow arrows. One of them in 2013 was a 'light-bulb' shaped CME (lower arrow) which remained tethered to the Sun (upper arrow). The extreme ultraviolet (from SDO/AIA) - eclipse composites show how critical these composites are for connecting the expanding CMEs back to the Sun. More curiously, however, are the features indicated by the white arrows in both 2012 and 2013. They are the indelible imprint produced by the passage of CMEs through the corona, prior to the eclipse. Cursory inspections limited to the LASCO/C2 coronagraph images, as seen in the composites of panels B and D, would have mistaken these

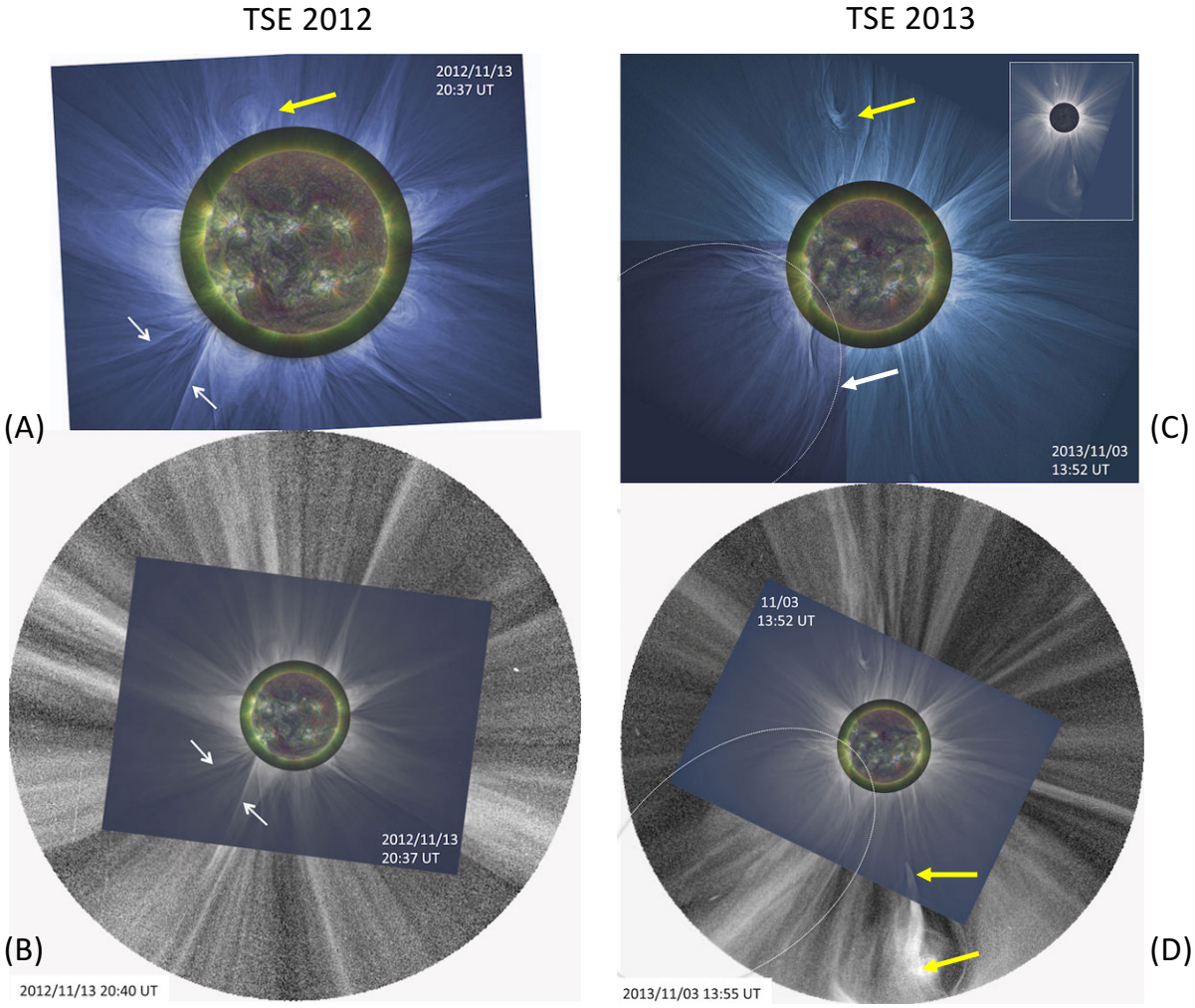

Figure 6. CMEs captured during the 2012 (A,B) and 2013 (C,D) total solar eclipses are indicated by the white arrows. Imprints of the passage of CMEs are shown by the yellow arrows and the large dashed curve in panels C and D. (See Alzate et al. 2017 for details.)

3. Temperature structure of the quiescent and dynamic corona

The heliocentric distance of 1 - 3 R_s, which we refer to in this work as the *inner corona*, is the most critical region where the plasma parameters defining the corona, including the magnetic

field, undergo their most pronounced changes. While white light images capture the intricate expansion of the magnetized coronal plasma, other diagnostic tools and observations are essential for exploring the physical properties of the plasma itself, such as the temperature, and elemental and ionic abundances of its major and minor constituents. Fortuitously, coronal forbidden lines emitting in the visible and near infrared offer unique diagnostic tools to exploit this region (see, e.g. Mason 1975, Habbal et al. 2007, 2010a, 2011, 2013; Judge et al., 2013; Landi et al, 2016; DelZanna & DeLuca 2018). In particular, the prevalence of emission from spectral lines from different charge states of the same element, with Fe being the most abundant, yields an unambiguous diagnostic of the electron temperature distribution in the corona, to name a few. Their diagnostic potential derives from their emission process, which is dominated by radiative excitation. This property enables the emission to often extend beyond the inner corona. This distance range significantly exceeds the spatial span of EUV emission, which is dominated by collisional excitation, and is limited to 1.25 R_s for the SDO/AIA data.

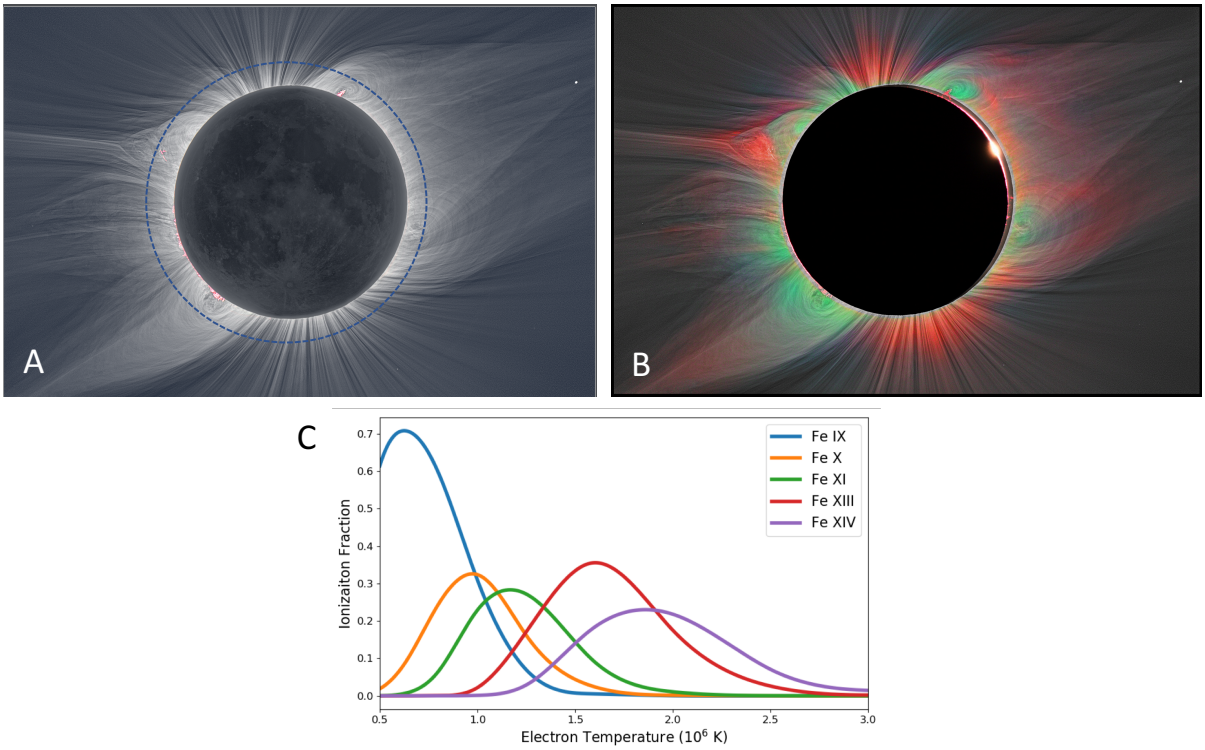

Figure 7. Images of the corona from the 1 August 2008 total solar eclipse in (A) white light, (B) Fe XI (red), Fe XIV (green) and white light (grey) composite. The dashed circle in (A) represents the extent of the field of view of the SDO/AIA EUV instrument. The white light image was taken by P. Aniol, M. Druckmüller, M. Dietzel and V. Rusin from Mongolia. The multi-wavelength observations were made by S. Habbal's team from the Gobi desert in China. (C) Plot of the ionization fraction of a suite of Fe lines covering 430 to 1015 nm, with data taken from Arnaud and Raymond (1992).

Shown in Fig. 7 is an example of processed images taken during the 1 August 2008 total solar eclipse in white light (A), and in emission from Fe XI at 789.2 nm and Fe XIV at 530.3 nm, overlaid over white light (B) (see Habbal et al., 2010a). This figure underscores a few outstanding features of eclipse multi-wavelength imaging. (1) As noted earlier, emission in white light extends to the edge of the field of view of 3 - 4 R_s. The dashed circle in Fig. 7A

outlines the extent of the field of view of the SDO/AIA EUV emission. The difference between the two fields of view underscores the importance of the spatial extent of the eclipse observations for capturing the expansion of different coronal structures away from the Sun. (2) Fe XI and Fe XIV emission extend to the edge of the same field of view.

The curves of ionization fraction for ionization equilibrium as a function of temperature, for the suite of Fe forbidden coronal emission lines, from Fe IX through Fe XIV, shown in Fig. 7c, are particularly valuable to appreciate their diagnostic potential. (Note that Fe XII is missing because its emission has a wavelength that falls close to the ultraviolet, and is more challenging to acquire from the ground.) This figure shows that the peak for each ion corresponds to a well-defined temperature. Given that the peaks for Fe XI and Fe XIV are very well separated, emission from these two lines, as shown in Fig. 7b, yields distinct structures in each, with open field structures dominated by the cooler Fe XI (with a peak at 1.2 MK), while closed field structures are dominated by Fe XIV emission (with a peak at 1.8 MK). It is thus clear from these examples, that the inner corona (and beyond) is multi-thermal, and that traces of the different temperature strands, revealed by emission from the distinct peak ionization temperatures of the Fe coronal forbidden lines, shown in Fig. 7c, are real.

Furthermore, knowledge of the ionization fraction of the different observed ions enables the reconstruction of maps of coronal electron temperature, as shown in the example of Fig. 8 from the total solar eclipse of 2017. The Sun was at the descending phase of activity, yet it is clear that the electron temperature distribution is bimodal, with the edges of the streamers reaching 1.5 MK, and coronal holes dominated by 1.2 MK plasmas. The map to the right shows the relative abundance of Fe^{13+} and Fe^{10+}, with the maximum occurring in the closed structures within the bulge of streamers.

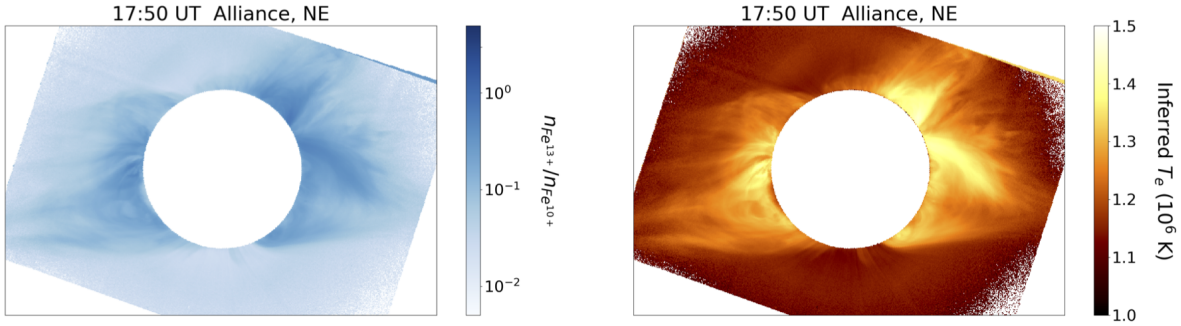

Figure 8. Distribution of the Fe^{+11} to Fe^{+13} abundance ratio (left) and of the inferred electron temperature (right) in the corona, from the 2017 total solar eclipse observations. (See Boe et al. 2020b for details.)

Just like the identification of the thermal environment of prominences was possible with multi-wavelength observations (e.g. Fig. 5A), so is the characterization of the thermal properties of a CME, as shown in Fig. 9. The fortuitous passage of two CMEs through the corona shortly before totality during the 2017 total solar eclipse (arrow A), and a few hours prior to totality (arrow B), enabled the multi-wavelength Fe XI - Fe XIV observations in Fig. 9b to show, for the first time, that CMEs are dominated by the hottest material (green in these images) in the corona. This comes as no surprise given that the hot prominence shrouds (shown in Fig. 5A), form the bulk of the CME fronts in most cases.

The 21 August 2017 total solar eclipse across the US also enabled multi-site observations, across several hundred miles. This geographic span corresponded to $\approx$ 30 minutes of eclipse time between the first and last observing site. Multi-wavelength observations with identical

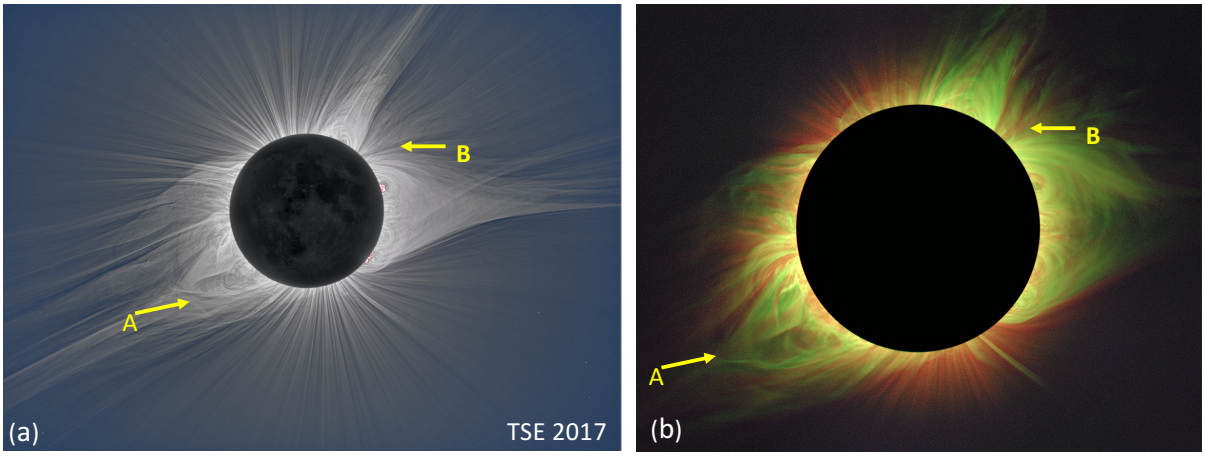

Figure 9. White light and multi-wavelength images of the corona during the 2017 total solar eclipse. The arrows point to the passage of CMEs during (east) and prior to (west) the eclipse.

instrumentation at three of the observing sites yielded temperature maps which revealed changes in the coronal temperature as a consequence of the passage of the CMEs. The example shown in Fig. 10 is from the first and last site separated by 1200 km and 28 minutes in eclipse time. The change in T_e is given in the left panel, and the significance of the change in the right one. Within this almost half hour, the temperature in the innermost corona increased, while it decreased further away from the Sun. These are the first such observations of thermodynamic changes associated with the passage of a CME through the inner corona. (See Boe et al. 2020a for details.)

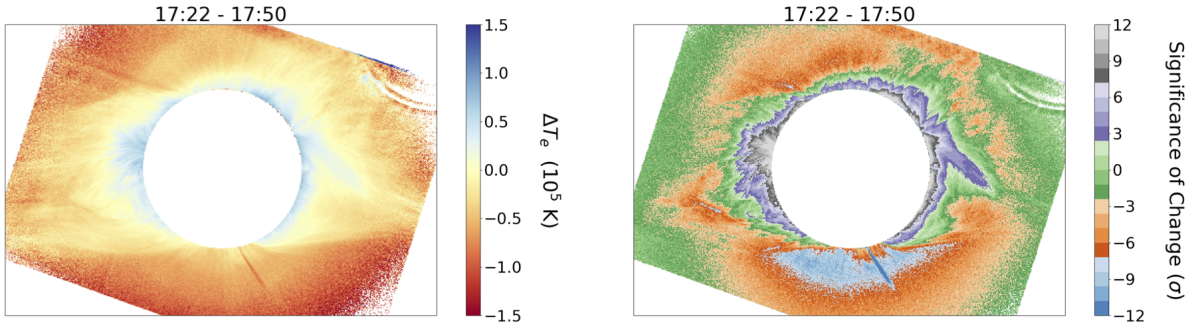

Figure 10. Changes in the coronal temperature following the passage of a CME through the corona (left). The right panel shows the statistical significance of these changes. The changes were inferred from multi-site multi-wavelength observations taken during the 2017 total solar eclipse. (See Boe et al. 2020a for details).

4. Empirical inference of the ion freeze-in distance

One of the key plasma parameters that has defied empirical inference is the ion freeze-in distance. This is the height above the solar surface at which collisions are not frequent enough to change a given ionization state. This distance is determined by the electron temperature and density. These parameters reflect the heating processes that shape the corona. Habbal et al. (2007, 2013) were the first to demonstrate that the freeze-in distance could be inferred empirically from

eclipse observations of emission from forbidden coronal lines and their underlying continuum. The technique was implemented in a comprehensive manner by Boe et al. (2018) who applied it to the 29 March 2015 total solar eclipse observations. The mapping of the freeze-in distance for two ions, namely the Fe^{10+} (blue) and Fe^{13+} (red) contours, is shown in Fig. 11. The difference in these contours demonstrates that the freeze-in distances are directly connected to the temperature and density distribution in the corona. They also show that the freeze-in distance is a lot closer to the solar surface than originally estimated by Ko et al. (1997), who used in-situ charge state measurements as boundary conditions for their inference.

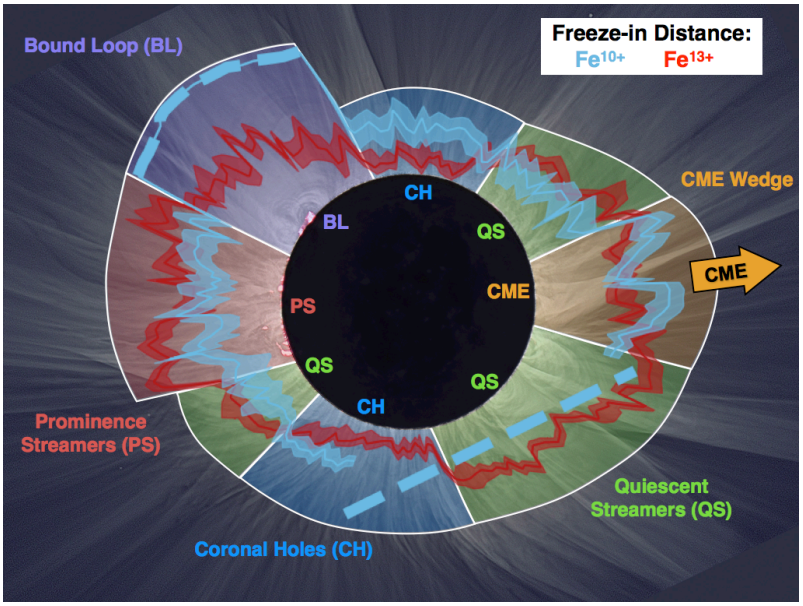

Figure 11. Overlay of the freeze-in distance for Fe^{10+} (blue) and Fe^{13+} (red) from the 2015 total solar eclipse observations over the corresponding white light image. The white bounding contours identify the different underlying structures in the corona, such as coronal holes and streamers, as well as a wedge associated with the passage of a CME. (See Boe et al., 2018 for details.)

5. Discovery of neutrals and low ionized elements in the inner corona

Multi-wavelength imaging is not the only tool for exploring the thermodynamics of the corona. Spectroscopy is another powerful tool as it captures not only the elemental and ionic composition of the corona, but mass motions, when present, through measurements of Doppler shifts. A dual channel partially multiplexed, two-dimensional imaging spectrometer was designed and built for eclipse observations (see Ding & Habbal 2017). The spectral observations obtained during the 20 March 2015 total solar eclipse led to the serendipitous discovery of a large number of spatially discrete Doppler-shifted fragments of Fe XIV 530.3 nm emission scattered across a projected area of $2.5 \times 1.3 R_s^2$ in the plane of the sky off the east limb of the Sun, as shown in Fig. 12. The speeds ranged from 100 to 1500 km/s. The different color-coded rectangles represent Doppler red-shifted plasma parcels moving away from the observer. The corresponding speeds are given in the legend on the right. The dominant emission was from Fe XIV, some accompanied by cool inclusions characterized by emission from neutral or low ionized elements typical of prominence material, shown by the red outline. This example is the first to capture the fate of eruptive prominence material as it leaves the coronal base. These are the first successful spectroscopic

observations to show that some of the erupting material in a prominence remains embedded in the filamentary CME front, without changing its ionization status, as the two expand in tandem into interplanetary space. Such a finding is corroborated by in-situ measurements of neutrals and low-ionized states of different elements in association with CMEs in interplanetary space (see, e.g. Gloeckler et al. 1999, Lepri and Zurbuchen 2010).

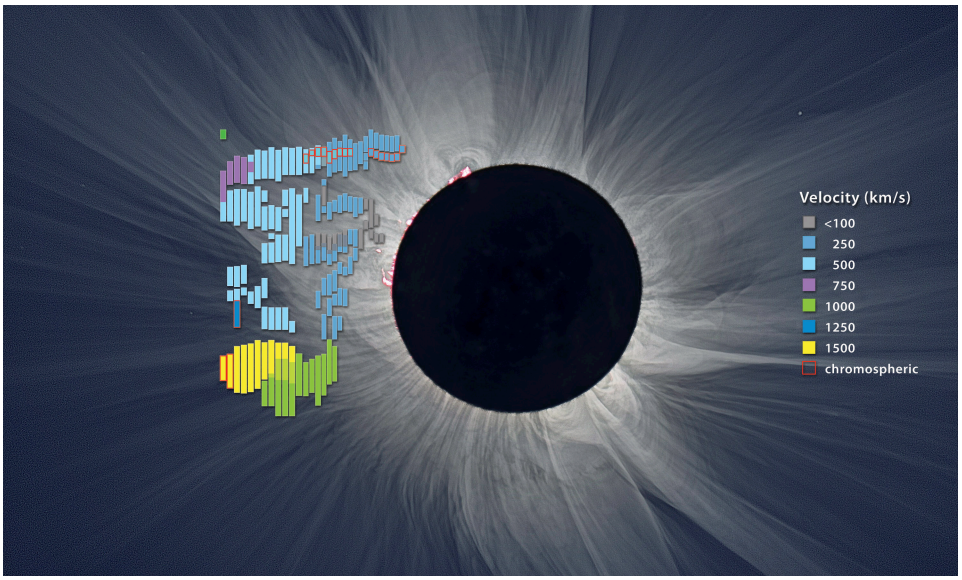

Figure 12. Map of Doppler shifted Fe XIV emission measured during the 29 March 2015 total solar eclipse, overlaid on the corresponding white light image of the corona. The color coding of the velocity of the red-shifted parcels is given in the legend on the right. The rectangles with a red border represent the plasma parcels accompanied by Doppler shifted cool chromospheric emission. (See Ding & Habbal 2017 for details.)

6. Conclusions

The eclipse observations presented here highlight their unique contribution to the exploration of the physics of the inner corona and the source regions of the solar wind. There are several factors that contribute to the unique insights gleaned from these observations: (1) their uninterrupted spatial coverage of the corona starting from the solar surface out to a few solar radii, and (2) the possibility to capture forbidden line emission in the visible during totality, and consequently, the corresponding rich diagnostic tools they offer. Most intriguing is the revelation that prominences are intrinsically associated with the most complex structures in the inner corona. They channel and initiate the dynamics of the magnetized coronal plasmas, which are manifested in a broad spectrum of plasma instabilities, most notable among them are CMEs. Their impact is not limited to the inner corona, as their cool remnants expand into interplanetary space unscathed, and the plasma instabilities they create also expand into interplanetary space, providing intriguing measurements for *Parker Solar Probe* and *Solar Orbiter*. Despite their paucity and short duration, total solar eclipse observations continue to offer an undeniably rich platform for exploring the signatures of coronal heating and solar wind acceleration processes.

Acknowledgments

The work presented here would not have been possible without the relentless efforts and dedication of the Solar Wind Sherpas who continue to travel across the world to collect

unique data during total solar eclipses. I would like to particularly acknowledge my long-time collaborator Judd Johnson with whom I observed my first total solar eclipse in 1995, and who continues to provide the critical technical expertise, savvy and sanity to the group. Martina Arndt, Huw Morgan, Adalbert Ding and Miloslav Druckmüller, who joined the Sherpas a few years later, added significantly to the scientific output of the eclipse observations. Younger, equally dedicated collaborators, who joined the ranks of the Sherpas about five years ago, include Nathalia Alzate, Jana Hoderóva, Pavel Štarha and Petr Štarha. Recent PhD students, namely, Ben Boe, Sage Constantinou, Michael Nassir and Bryan Yamashiro, are contributing significantly with fresh ideas and challenging intellectual insights. Their enthusiasm makes these expeditions, which can be grueling at times, worth the effort. Support for the more recent eclipse observations was provided by NSF grants AGS-1834662 and AST-1839436, and NASA grant NNX17AH69G, to the Institute for Astronomy of the University of Hawaii.

References

[1] Alzate, N, Habbal, S R, Druckmüller, M, Emmanouilidis, C, and Morgan, H 2017 Dynamics of large-scale coronal structures as imaged during the 2012 and 2013 total solar eclipses *ApJ* **848** 84
[2] Arnaud, J and Newkirk, G Jr 1987 Mean properties of the polarization of the Fe XIII 10747 A coronal emission line *A&A* **178** 263
[3] Arnaud, M and Raymond, J 1992 Iron ionization and recombination rates and ionization equilibrium *ApJ* **398** 394
[4] Boe, B, Habbal, S R and Druckmüller, M 2020b Coronal magnetic field topology from total solar eclipse observations *ApJ* in press
[5] Boe, B, Habbal, S R, Druckmüller, M, Ding, A, Hodérova, J, and Štarha, P 2020a CME-induced thermodynamic changes in the corona as inferred from Fe xi and Fe xiv emission observations during the 2017 August 21 total solar eclipse *ApJ* **888** 100
[6] Boe, B, Habbal, S R, Druckmüller, M, Ding, A, Landi, E, Kourkghi, E and Hutton, J 2018 The first empirical determination of the Fe^{10+} and Fe^{13+} freeze-in distances in the solar corona *ApJ* **859** 155
[7] Brueckner, G E et al. 1995 The Large Angle Spectroscopic Coronagraph (LASCO) *Sol. Phys* **162** 357
[8] Clark, S E, Peek, J E G and Putnam, M E 2014 Magnetically aligned H I fibers and the Rolling Hough Transform *ApJ* **789** 82
[9] Ding, A and Habbal, S R 2017 First detection of prominence material embedded within a 2 10^6 K CME front streaming away at 100-1500 km s^{-1} in the solar corona *ApJ* **842** L7
[10] Druckmüller, M, Habbal, S R, Alzate, N and Emmanouilidis, C 2017 Tethered prominence-CME systems captured during the 2012 November 13 and 2013 November 3 total solar eclipses. *ApJ* **851** L41
[11] Druckmüller, M, Habbal, S R, and Morgan, H 2014 Discovery of a new class of coronal structures in white light eclipse Images *ApJ* **785** 14
[12] Druckmüller, M 2009 Phase Correlation Method for the Alignment of Total Solar Eclipse Images *ApJ* **842L** 7D
[13] Druckmüller, M, Rusin, V and Minarovjech, M 2006 A new numerical method of total solar eclipse photography processing *CoSka* **36** 131
[14] Edlén, B 1945 The identification of the coronal lines (George Darwin Lecture) *MNRAS* **105** 323
[15] Gloeckler, G, et al. 1999 Unusual composition of the solar wind in the 2-3 May 1998 CME observed with SWICS on ACE *GeoRL* **26**, 157
[16] Grotrian, W 1939 Zur Frage der Deutung der Linien im Spektrum der Sonnenkorona *Die Naturwissenschaften* **27** 214
[17] Habbal, S R, Morgan, H, and Druckmüller, M 2014 Exploring the prominence-corona connection and its expansion into the outer corona using total solar eclipse observations *ApJ* **793** 119
[18] Habbal, S R, Ding, A, Cooper, J F, Daw, A and Sittler, E C 2013 Probing the fundamental physics of the solar corona with lunar solar occultation observations *Sol Phys* **285** 9
[19] Habbal, S R, Druckmüller, M, Morgan, H, Ding, A, Johnson, J, Druckmüllerová, H, Daw, A, Arndt, M B, Dietzel, M and Saken, J 2011 Thermodynamics of the solar corona and evolution of the solar magnetic field as inferred from the total solar eclipse observations of 2010 July 11 *ApJ* **734** 120
[20] Habbal, S R, Druckmüller, M, Morgan, H, Scholl, I, Rušin, V, Daw, A, Johnson, J and Arndt, M 2010c Total solar eclipse observations of hot prominence shrouds *ApJ* **719** 1362
[21] Habbal, S R, Morgan, H, Druckmüller, M, and Ding, A 2010b On the constancy of the electron temperature in the expanding corona throughout solar cycle 23 *ApJ* **711** L75
[22] Habbal, S R, Druckmüller, M, Morgan, Daw, A, Johnson, J, Ding, A, Arndt, M, Esser, R, Rušin, V and

Scholl, I 2010a Mapping the distribution of electron temperature and Fe charge states in the corona with total solar eclipse observations *ApJ* **708** 1650
[23] Habbal, S R, Morgan, H, Johnson, J, Arndt, M B, Daw, A, Jaeggli, S, Kuhn, J and Mickey, D 2007 Localized enhancements of Fe^{+10} density in the corona as observed in Fe XI 789.2 nm during the 2006 March 29 total solar eclipse *ApJ* **663** 598
[24] Judge, P G, Habbal, S R and Landi, E 2013 From forbidden coronal lines to meaningful coronal magnetic fields *Sol. Phys* **288** 467
[25] Ko, K-Y, Fisk, L, Geiss, J, Gloeckler, G and Guhathakurta, M 1997 An empirical study of the electron temperature and heavy ion velocities in the south polar coronal hole *Sol. Phys.* **171** 345
[26] Landi, E, Habbal, S R and Tomczyk, S 2016 Coronal plasma diagnostics from ground-based observations *JGR* **121** 8237
[27] Lepri, S and Zurbuchen, T H 2010 Direct observational evidence of filament material within interplanetary coronal mass ejections *ApJL* **723**, L22
[28] Lyot, B 1932 Etude de la couronne solaire en dehors des eclipses *ZA* **5** 73
[29] Mason, H E 1975 The excitation of several iron and calcium lines in the visible spectrum of the solar corona *MNRAS* **170** 651
[30] Maunder, E W 1899 The Indian Eclipse, 1898: Report of the expeditions organized by the British Astronomical Association to observe the total solar eclipse of 1898 January 22
[31] Miloch, W J, Habbal, S R and Esser, R 2012 Plasma dynamics at the prominence—corona interface *ApJ* **752** 85
[32] Neugebauer, M and Schneider, C W 1966 Mariner 2 Observations of the Solar Wind, 1, Average Properties *JGR* **71** 4469
[33] Parker, E 1958 *ApJ* Dynamics of the Interplanetary Gas and Magnetic Fields **128** 664
[34] Young, C A 1872 The corona line *Nature* **7** 28
[35] Young, C A 1871 The solar spectrum *Nature* **4** 445
[36] Young, C A 1870 The American eclipse *Nature* **1** 532